# Interference without an interferometer: a different approach to measuring, compressing, and shaping ultrashort laser pulses

**Yves Coello,[1] Vadim V. Lozovoy,[1] Tissa C. Gunaratne,[1] Bingwei Xu,[1] Ian Borukhovich,[2] Chien-hung Tseng,[2] Thomas Weinacht,[2] and Marcos Dantus[1,3,*]**

[1]*Department of Chemistry, Michigan State University, East Lansing, Michigan 48824, USA*
[2]*Department of Physics, Stony Brook University, Stony Brook, New York 11794, USA*
[3]*Department of Physics and Astronomy, Michigan State University, East Lansing, Michigan 48824, USA*
**Corresponding author: dantus@msu.edu*

Received November 2, 2007; revised February 15, 2008; accepted March 11, 2008;
posted April 21, 2008 (Doc. ID 89325); published May 30, 2008

The inherent brevity of ultrashort laser pulses prevents a direct measurement of their electric field as a function of time; therefore different approaches based on autocorrelation have been used to characterize them. We present a discussion, guided by experimental studies, regarding accurate measurement, compression, and shaping of ultrashort laser pulses without autocorrelation or interferometry. Our approach based on phase shaping, multiphoton intrapulse interference phase scan, provides a direct measurement of the spectral phase. Illustrations of this method include new results demonstrating wavelength independence, compatibility with sub-5 fs pulses, and a perfect match for experimental coherent control and biomedical imaging applications.

*OCIS codes:* 320.0320, 320.7100.

## 1. INTRODUCTION

Pulse compression, shaping, and characterization at the laser target are of critical importance to ensure reproducible femtosecond laser applications that now include biomedical imaging, metrology, micromachining, analytical chemistry, material processing, photodynamic therapy, surgery, and even dentistry. In principle, the Fourier transform of the ultrashort electromagnetic pulse spectrum provides its temporal duration. This statement is accurate when the pulse is transform-limited (TL), i.e., all frequency components in its bandwidth have the same phase. The actual pulse duration of ultrashort pulses is always greater than that of the TL pulse because of phase distortions that arise from optics and from transmission through any medium other than vacuum. Here we use the ratio $\tau/\tau_{TL}$ as a parameter to characterize the quality of the pulse, where $\tau$ and $\tau_{TL}$ are the time durations of the measured and TL pulses, respectively. Strictly speaking, root-mean-square time durations should be used for $\tau$; however, the generalized approach is to use the FWHM time duration for simplicity. The $\tau/\tau_{TL}$ parameter is similar to the $M^2$ parameter used in optical design, giving the ratio between the measured value versus the theoretical optimum. Typical values for $\tau/\tau_{TL}$ range from 1.1 for well-tuned systems to less than 1.5 for most advertised commercial systems and finally from 10 to 100 when pulses are broadened by optics, such as high-numerical-aperture microscope objectives.

Ultrashort pulse broadening is a serious problem affecting every application. One can divide approaches to dealing with it into two broad categories: direct compression and phase measurement followed by compensation. For the former approach, phase distortions are minimized without being measured; the latter depends on an accurate phase measurement followed by accurate compensation. The most common approaches to pulse compression are schematically illustrated in Figs. 1(a)–1(c). The early incorporation of compressors consisting of gratings, prisms, and their combination led to great advancements in femtosecond technology during the early 1980s, culminating in the production of 6 fs pulses [1]. This approach, which requires one or more laser experts, is illustrated in Fig. 1(a). A second characterization-free approach uses a computer-controlled pulse shaper and an optimization algorithm that takes the integrated second harmonic generation (SHG) intensity from the laser pulses as the feedback in a closed loop [2,3] as illustrated in Fig. 1(b). In both of these characterization-free cases, success depends on the noise level of the laser system. The pulse-to-pulse stability of the SHG output is typically 2%–6%, assuming laser fluctuations of 1%–3% in the fundamental. Because $\tau/\tau_{TL}=I_{SHG\text{-}TL}/I_{SHG}$, measurement-free approaches could reach $\tau/\tau_{TL}$ values as low as 1.02–1.06 provided the algorithm is given sufficient time to converge. For many cases this level of performance is sufficient, and using a prism–grating compressor or even a simple uncalibrated pulse shaper with feedback will accomplish the task.

If $\tau/\tau_{TL}<1.1$ is consistently required, such as when the ultrashort pulses are used to study optical properties of materials, an actual measurement of the pulses is required. The most simple situation arises when well-characterized pulses, such as TL pulses, are used for measuring phase-distorted pulses. In this situation, the unknown phase distortions can be calculated from the in-

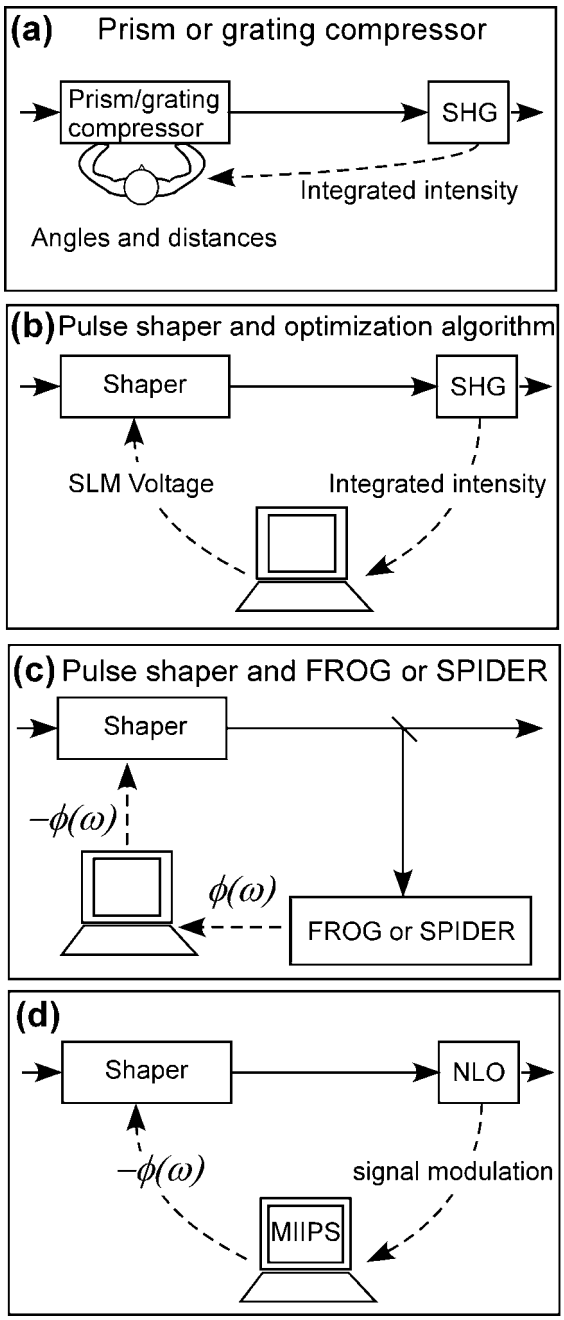


Fig. 1. Pulse compression approaches. (a) Manual prism–grating compressor adjustment. (b) Optimization algorithm using the SHG signal as feedback. These two approaches do not require spectral phase measurements. (c) Measurement and correction using FROG or SPIDER as the characterization technique. (d) MIIPS. Measurement and correction are seamlessly integrated in a compact setup. NLO, nonlinear optical medium.

terferogram between the unknown and the reference pulses. Unfortunately, well-characterized pulses are not usually available. It has also been theoretically and experimentally shown that, through an iterative algorithm, one can determine the pulse field from a fringe resolved autocorrelation and the spectrum of the pulse [4]. However, this algorithm is rarely used. A more common approach is to retrieve the unknown phase using an autocorrelator- or interferometer-based technique such as frequency resolved optical gating (FROG) [5,6] or spectral phase interferometry for direct electric-field reconstruction (SPIDER) [7,8], and to use the knowledge of the retrieved phase and a calibrated pulse shaper for pulse compression [9–12]. This approach is illustrated in Fig. 1(c).

In this paper we discuss a different approach, called multiphoton intrapulse interference phase scan (MIIPS) [13–16], to accurately measure and correct the unknown phase distortions of the pulses while avoiding the use of autocorrelation or interferometry as illustrated in Fig. 1(d). In Section 2 we present the principles and theory that describe different approaches to MIIPS and discuss some of its limitations. In Section 3 we describe a number of applications starting with pulse characterization and compression of sub-5 fs pulses, MIIPS without an adaptive pulse shaper, high intensity sub-5 fs pulse characterization and compression, and measurement and correction of the spectral phase distortions introduced by high-numerical-aperture microscope objectives. We also describe accurate spectral phase measurements, such as the group-velocity dispersion (GVD) of water, the phase distortions introduced by scattering biological tissue, and the measurement of arbitrarily complex phases. We present MIIPS measurements from other nonlinear optical (NLO) signals, such as SHG in surface plasma, third harmonic generation in air, and self-diffraction (SD) in transparent media. We also demonstrate accurate pulse shaping as required for standoff sensing applications. In Section 4 we present a number of pulse shaper assisted spectral phase characterization methods that are achieved by the same setup and discuss their individual advantages. Finally, we present our conclusions in Section 5.

## 2. MIIPS

We start our discussion by remembering the effect of the different terms of a Taylor expansion of the spectral phase $\phi(\omega)$ on the time profile of an ultrashort pulse,

$$\phi(\omega) = \phi_0 + \phi_1(\omega - \omega_0) + \tfrac{1}{2}\phi_2(\omega - \omega_0)^2 + \tfrac{1}{6}\phi_3(\omega - \omega_0)^3 \cdots . \quad (1)$$

The zeroth order phase $\phi_0$ (sometimes called absolute phase) determines the relative position of the carrier wave with respect to the pulse envelope. In most cases, the $\phi_0$ term is of little interest. This is due to the fact that when the pulse is many carrier-wave cycles long, which is the most common situation, a change in $\phi_0$ has a very small effect on the pulse field. None of the pulse characterization methods mentioned in this paper are able to measure the zeroth order phase. The first order phase $\phi_1$ corresponds to a shift of the pulse envelope in time. Given that the interest is typically centered on the pulse shape and not on the arrival time of the pulse, the $\phi_1$ term is also of little interest. The second and higher order terms do have an effect on the time profile of the pulses. From the discussion herein, it becomes clear that the second derivative of the spectral phase $\phi''(\omega)$ is the parameter that determines the pulse shape.

MIIPS measures $\phi''(\omega)$ by successively imposing a set of parameterized ($p$) reference spectral phases $-f(\omega,p)$ to the pulses with unknown phase distortion $\phi(\omega)$ and ac-

quiring the corresponding NLO spectra, for example SHG. In the second derivative space, the set of reference functions $f''(\omega,p)$ can be visualized as a grid used to map the unknown $\phi''(\omega)$, i.e., to find which $f''(\omega,p)$ intersects $\phi''(\omega)$ at any desired frequency $\omega_i$;

$$\phi''(\omega_i) = f''(\omega_i, p_{\max}). \tag{2}$$

Note that, for each such point the reference function cancels the local chirp and, therefore, the NLO signal is maximized at $\omega_i$; hence the required parameter is labeled $p_{\max}$. Multiphoton intrapulse interference (MII) [17,18] is at the heart of MIIPS and explains why Eq. (2) is satisfied [16].

The most simple grid for mapping the unknown second derivative of the phase consists of constant functions $f''(\omega,p)=p$ [Fig. 2(a)] [19], which correspond to linear chirp. In this case, different amounts of linear chirp can be imposed on the pulses using passive or adaptive optics (see Subsection A.2). For each reference phase, an NLO spectrum is plotted as a function of $p$ in a two dimensional contour map [Fig. 2(b)]. The feature of interest is $p_{\max}(\omega)$, which can be visualized by drawing a line through the maxima in the contour plot [solid curve in Fig. 2(b)]. The spectral phase information is directly obtained by finding $p_{\max}(\omega)$ and using Eq. (2). In the case of chirp MIIPS, Eq. (2) reads $\phi''(\omega)=f''(\omega,p_{\max})=p_{\max}(\omega)$. Therefore, the unknown $\phi''(\omega)$ is directly obtained from the contour plot without any mathematical retrieval procedure as shown in Fig. 2(b) [19].

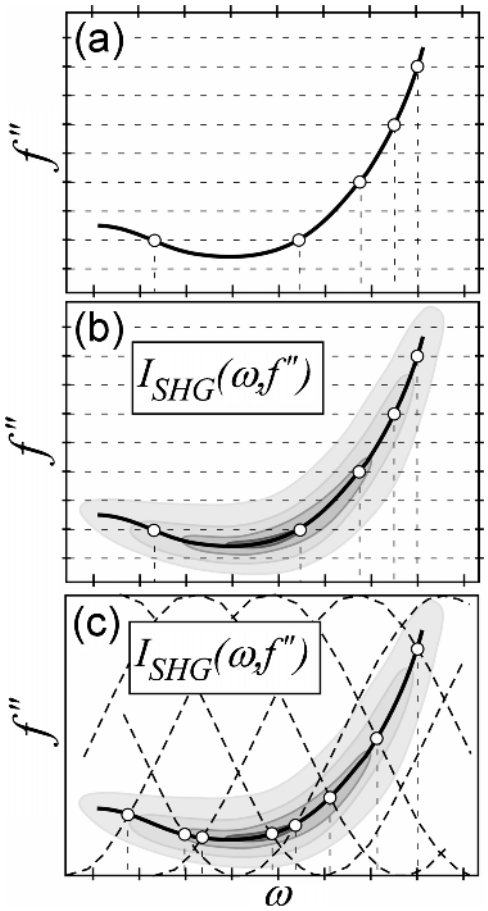


Fig. 2. Principle of MIIPS. A set of reference functions $f''(\omega,p)$ provides a reference grid that is used to map the unknown $\phi''(\omega)$. (a) Conceptual diagram based on a horizontal reference grid (dashed lines) corresponding to different amounts of linear chirp. The solid curve represents the unknown $\phi''(\omega)$. (b) MIIPS trace corresponding to a horizontal grid. (c) MIIPS trace corresponding to a sinusoidal grid. Note that in both cases the unknown $\phi''(\omega)$ is directly revealed by the contour plot.

If an adaptive pulse shaper is used, the number of possible reference functions that can be used is unlimited. Sinusoidal reference spectral phases $f(\omega,\delta) = \alpha \sin[\gamma(\omega-\omega_0)-\delta]$, where $\delta$ is a parameter scanned across a $4\pi$ range, have been extensively used [14–16]. When the NLO signal is plotted as a function of $\omega$ and $f''(\omega,p)$, the results obtained from applying any type of reference phase function reveal the unknown $\phi''(\omega)$ by finding the line that goes through the maxima in the contour plot. Note that the dashed lines in Fig. 2(c) correspond to the second derivative of the sinusoidal reference functions, $f''(\omega,\delta)=-\alpha\gamma^2 \sin[\gamma(\omega-\omega_0)-\delta]$ and that the maximum NLO signal occurs at the points at which a reference function intersects the unknown $\phi''(\omega)$. The NLO spectrum can also be plotted as a function of $\delta$. In this case, diagonal parallel straight lines separated by $\pi$ are obtained for $\delta_{\max}(\omega)$ when the pulses are TL [14,20]. Additional group delay dispersion (GDD) causes a change in the spacing between the curves, and third order dispersion (TOD) causes a change in the inclination of these curves [14,21]. In both cases, the changes are proportional to the magnitude and sign of the dispersion. The sinusoidal MIIPS approach has been described in great detail in [16,20]. Experimental data illustrating the rigorous measurement of $\phi''(\omega)$ using both chirp and sinusoidal MIIPS are presented in this paper.

A MIIPS scan takes between 5 and 15 s depending on the device used to introduce the reference phases and the number of phases used. Although not necessary, an iterative measurement-compensation routine can be used to achieve the maximum possible accuracy, especially in the case of complex spectral phases [16,19,20]. Double integration of the measured $\phi''(\omega)$ results in $\phi(\omega)$. Once $\phi(\omega)$ is obtained, the introduction of $-\phi(\omega)$ by the shaper eliminates the measured phase distortions to achieve TL pulses. A comprehensive analysis of the precision and accuracy of MIIPS was carried out in 2006 [16]. Using MIIPS, $\tau/\tau_{\mathrm{TL}}$ values routinely reach the 1.01 level and in some cases are even lower than 1.001.

The greatest challenge in ultrashort pulse characterization is the accurate measurement of abrupt (discontinuous) phase changes that may be introduced by pulse shapers and to some extent by dielectric optics. Phase measurements near such a discontinuity are problematic. The curvature of the phase changes that can be measured by MIIPS increases with the optical resolution of the pulse shaper being used. For example, a $\pi$-phase step to be accurately measured using 10 or 100 nm FWHM pulses and a 640 pixel pulse shaper should have a run longer than 0.15 or 1.5 nm, respectively. Another issue worth mentioning here is that the minimum amount of chirp that can be measured increases for narrower bandwidths [19]. For example, the uncertainty of a $\phi''(\omega)$ measurement for pulses spanning 10 or 100 nm FWHM would be $\sim\pm 500$ or $\pm 5$ fs$^2$, respectively. When MIIPS is implemented by using a spatial light modulator (SLM)-based

pulse shaper, the maximum phase delay that can be introduced limits the measurable phase range. By phase wrapping and double passing the SLM, maximum delays of up to 1000 rad are possible.

## 3. MIIPS APPLICATIONS

### A. Pulse Characterization and Compression

*1. Sub-5 fs Laser Pulses*

The ability to measure and correct the spectral phase of a femtosecond laser becomes more challenging as the spectral bandwidth increases. Characterization and compression of sub-5 fs pulses have been reported using second harmonic generation-frequency resolved optical gating (SHG-FROG) [22], SPIDER [23,24], and MIIPS [25]. The characterization and compression of sub-5 fs pulses using MIIPS is illustrated in Fig. 3(a). The spectral phase of the pulses was corrected to within 0.1 rad accuracy across the entire bandwidth [Fig. 3(a), top panel]. For these measurements, the SHG spectrum was obtained from a 20 $\mu$m thick KDP crystal. The calculated FWHM time duration of the compressed pulses was 4.3 fs [Fig. 3(a), inset]. The resulting TL pulses generated the SHG spectrum shown in Fig. 3(b), the broadest UV spectrum to date obtained by direct conversion using a nonlinear crystal.

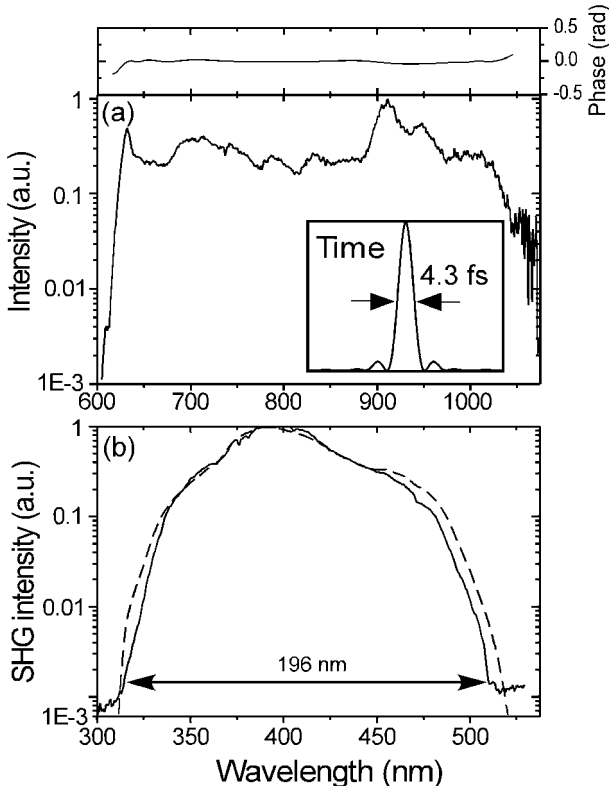


Fig. 3. MIIPS spectral phase correction of sub-5 fs laser pulses. (a) Spectrum of the ultrabroad-bandwidth pulses compressed with MIIPS. The spectral phase was corrected within 0.1 rad accuracy across the whole bandwidth [top panel in (a)]. The time profile of the compressed pulses is shown in the inset. The FWHM is 4.3 fs. (b) Measured (solid curve) and Fourier transform calculated (dashed curve) SHG spectra of the pulses after compression. The response function of the crystal was not considered in the calculation.

*2. MIIPS Without an Adaptive Pulse Shaper*

In this new development, we demonstrate MIIPS spectral phase measurements without the use of an adaptive pulse shaper. Instead, the reference functions $f''(\omega,p)$ are introduced using standard passive optics, such as a prism-, grating-, or prism-pair arrangement. In this experiment, different amounts of linear chirp were introduced to amplified pulses using the built-in compressor in the regenerative amplifier by varying the spacing between the grating pair. As explained in Section 2 and illustrated in Fig. 2(b), the measured $\phi''(\omega)$ is directly visualized in the chirp MIIPS trace shown in Fig. 4. The linear $\phi''(\omega)$ dependence indicates the presence of a cubic phase distortion, also known as TOD. No effort was made here to eliminate the measured TOD.

*3. High Intensity Sub-5 fs Pulse Characterization and Compression*

Intense sub-10 fs laser pulses are required in high-field laser science for applications, such as single attosecond pulse generation [26]. Because of spectral narrowing in the amplification process, the shortest pulses that can be obtained from a Ti:sapphire-based chirped-pulse amplification (CPA) system are usually limited to ~15 fs [27]. A common technique for generating intense few-cycle laser pulses is by compression of the continuum generated by self-phase modulation in a rare-gas filled hollow-core fiber [28,29]. Spectral phase characterization of such pulses has been reported using SHG-FROG [30]. Adaptive phase characterization and correction have been accomplished using *M*-SPIDER and an SLM-based pulse shaper [23], and more recently using MIIPS [31]. Figure 5(a) shows the spectrum and the spectral phase of continuum generated in an Ar-filled hollow-core fiber characterized by MIIPS. The time duration of the laser pulses was 166 and 4.8 fs before and after MIIPS compression, respectively

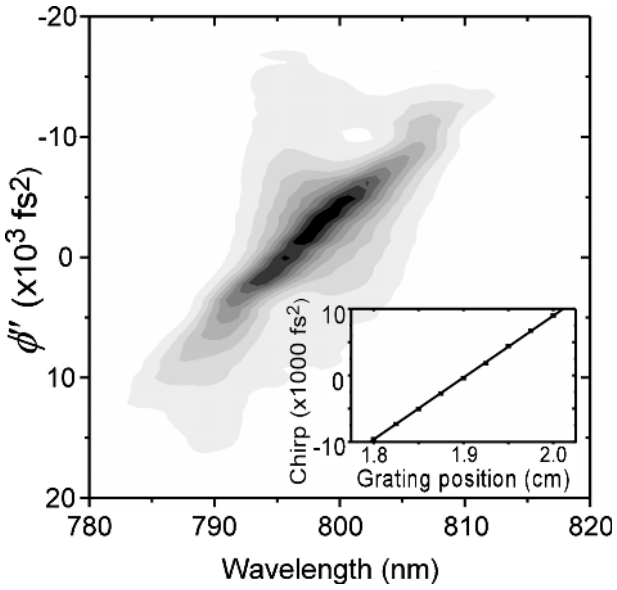


Fig. 4. MIIPS spectral phase measurement with a compressor. The chirp MIIPS trace for amplified laser pulses obtained using the built-in compressor in the regenerative amplifier is shown. The linear $\phi''(\omega)$ feature revealed by the trace corresponds to a cubic spectral phase distortion. The inset shows how linear chirp depends on the grating position for our compressor.

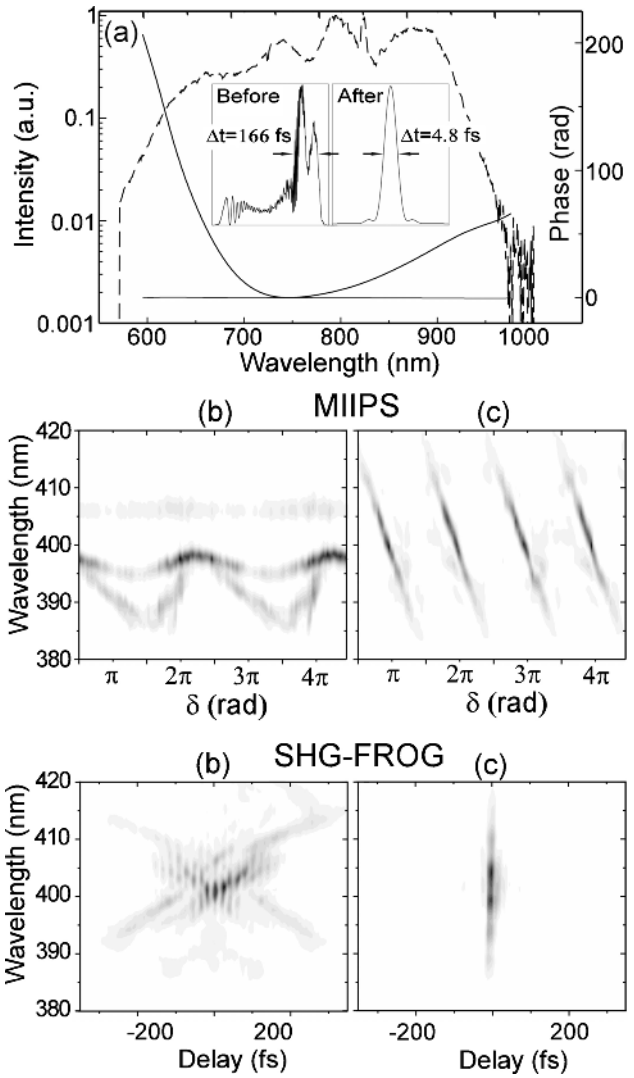


Fig. 5. MIIPS compression of continuum generated in an Ar-filled hollow-core fiber. (a) Spectrum (dashed curve) and phase (solid curve) of the continuum together with the temporal profile (inset) before and after spectral phase correction. MIIPS and SHG-FROG traces of pulses (b) before and (c) after MIIPS compression are shown. These pulses were obtained by blocking part of the continuum spectrum shown in (a) at the Fourier plane of the pulse shaper (see text). The parallel features in the (c) MIIPS trace indicate TL pulses. The remaining subpulses in the (c) SHG-FROG trace are a result of the deeply modulated spectrum.

(inset). The pulse energy of the compressed pulses was ~150 $\mu$J/pulse. The phase-corrected continuum has successfully been used for the remote detection of chemicals [31]. For this application, part of the spectrum was blocked at the Fourier plane of the pulse shaper. Figures 5(b) and 5(c) show a comparison of MIIPS and SHG-FROG traces of such pulses before and after MIIPS compression.

*4. Measurement and Correction of Spectral Phase Distortions Introduced by High-Numerical-Aperture Objectives*

An important obstacle in the development of two-photon microscopy with ultrashort pulses (<50 fs) has been the significant amount of phase distortions that high-numerical-aperture objective lenses introduce. Compensation of the quadratic term of the distortions is routinely accomplished using a prism precompressor. However, higher order phase distortions introduced by the objective and even by the prisms used for precompression cannot be corrected by this method (Fig. 6). Measurements of spectral phase distortions introduced by objectives have been obtained using FROG [32,33] and MIIPS [16] for NAs up to 1.25 and 1.45, respectively. As a result of the MIIPS spectral phase correction, numerous advantages for two-photon microscopy have been demonstrated, including higher fluorescence intensity as illustrated in Fig. 6, deeper sample penetration, improved signal-to-noise ratio, and less photobleaching. These advantages are not observed if only quadratic dispersion is compensated for while higher order dispersion is not [34].

### B. Accurate Spectral Phase Measurements

*1. Group-Velocity Dispersion of Water Measured with* $0.2\ \mathrm{fs}^2/\mathrm{mm}$ *Accuracy*

Knowledge of the dispersive properties of optical media is of great importance for femtosecond laser applications. The second order dispersion $k''$, commonly referred to as GVD, is an especially critical parameter because it determines the temporal broadening experienced by ultrashort pulses after traveling through a material. GVD measurements of water and seawater have been obtained using MIIPS [21] with an accuracy comparable only to that of white-light interferometry [35]. The measurements were carried out by transmitting an ultrabroad-bandwidth femtosecond laser (620–1025 nm) through water-containing cuvettes with 5, 10, 20, and 30 mm path lengths. In each case, MIIPS directly measured the GDD

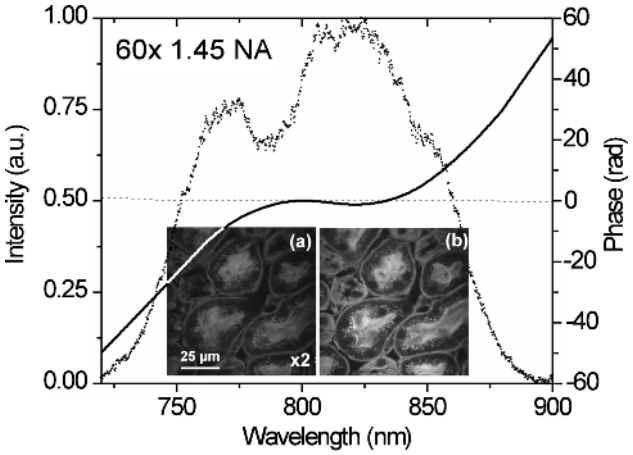


Fig. 6. MIIPS characterization and compensation of spectral phase distortions introduced by an oil-immersion 60×1.45 NA objective. Spectral phase distortions (solid curve) remaining after prism-pair precompression in 100 nm bandwidth pulses (dotted line, spectrum) that have been focused with the objective. Note that the remaining phase is mainly cubic because precompression eliminates the quadratic but not the higher order phase terms. After MIIPS correction, the spectral phase is flat (dashed curve). The inset shows a comparison of two-photon excitation microscopy images of a kidney sample slide (a) when only the precompressor is used, and (b) when MIIPS phase compensation is applied. To allow for direct visual comparison of the images, the intensity of the precompressor-only image was enhanced by a factor of 2 (2×). As a result of MIIPS correction of cubic and higher order phase terms, the average intensity of the image increased five times.

introduced by the sample, and from the slope of a linear fit to the data as a function of path length, a measurement of $k''$ was obtained. The results obtained are in very good agreement with calculated values based on the knowledge of the refractive index of water as a function of frequency [36,37] as shown in Fig. 7(a). The deviation between the MIIPS measurements and the calculations based on the Sellmeier model [37] is smaller than $\pm 0.2\ \mathrm{fs}^2/\mathrm{mm}$ within the measured wavelength range. Furthermore, the $\pm 0.2\ \mathrm{fs}^2/\mathrm{mm}$ accuracy and a $\pm 0.1\ \mathrm{fs}^2/\mathrm{mm}$ precision obtained with MIIPS allowed for detecting a $\sim 1.3\ \mathrm{fs}^2/\mathrm{mm}$ difference between the GVD of deionized water and that of seawater [Fig. 7(b)].

### *2. Spectral Phase Measurements Through Scattering Biological Tissue*

One of the most popular applications for femtosecond laser pulses is nonlinear biomedical imaging. Methods such as two-photon microscopy take advantage of the ability of near-IR lasers to travel through scattering biological tissue and provide high-resolution images [38]. The development of techniques for optimized depth-resolved imaging, as well as surgical procedures involving femtosecond lasers, will require accurate characterization of pulses after they transmit through biological samples. After propagation through scattering biological tissue, the majority of the beam is scattered making it impossible to use pulse characterization methods that depend on overlapping two or more pulses. Pulse characterization through scattering biological tissue is an illustrative example of the MIIPS performance regardless of beam-mode quality. Spectral phase characterization has been shown after the pulses traveled through a 1 mm thick chicken breast tissue slice [39] and a cow-eye cornea-lens complex [21]. A comparison of the spectral phase before and after the pulses traveled through the chicken breast tissue slice is shown in Fig. 8(a), together with the corresponding MIIPS traces. The GDD introduced by a cow cornea-lens complex squeezed to ~5 mm in thickness is shown in Fig. 8(b).

It is worthwhile to discuss the effect of noise on a MIIPS measurement. We begin by discussing the noise from the source (pulse-to-pulse and mode quality). Through the use of averaging, the influence of pulse-to-pulse fluctua-

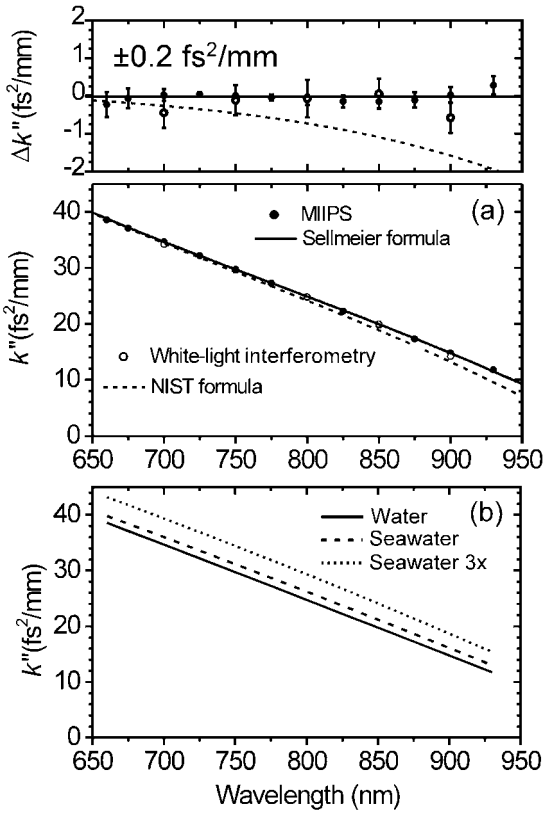


Fig. 7. MIIPS accurate GVD measurements. (a) Comparison of $k''$ values for water obtained using MIIPS and white-light interferometry and calculated using the National Institute of Standards and Technology (NIST) [36] and Sellmeier formulas for the refractive index of water. While MIIPS measurements provide a continuous function for $k''$, here we only plot values every 25 nm. The top panel shows the deviation of the corresponding values with respect to those calculated using the Sellmeier model. Note that for the MIIPS measurements, this deviation is not greater than $0.2\ \mathrm{fs}^2/\mathrm{mm}$. (b) $k''$ measurements of water, seawater, and seawater with three times the concentration of salt in seawater ($3\times$). The accuracy and precision of MIIPS allowed us to detect a linear increase in $k''$ as a function of the increasing concentration of sea salt.

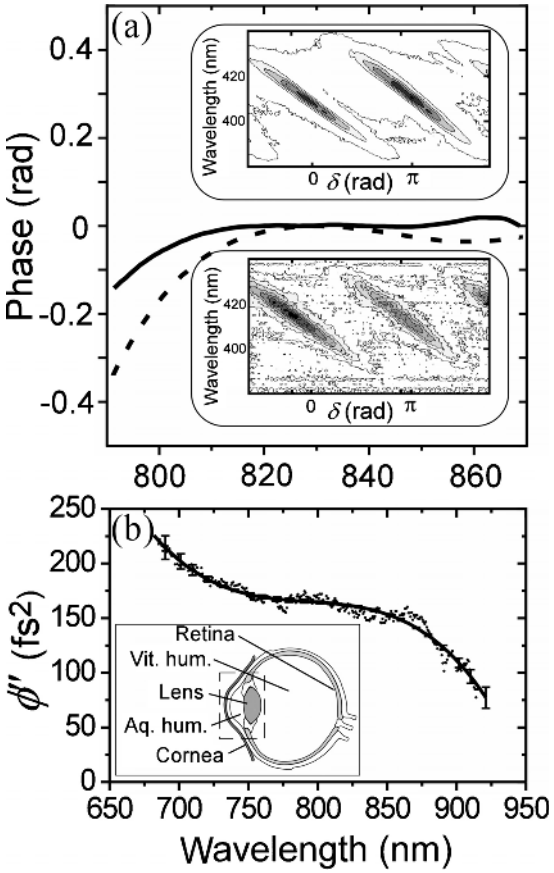


Fig. 8. MIIPS measurements through biological tissue. (a) Spectral phase measurement before (solid curve) and after (dashed curve) the pulses transmit through a 1 mm thick chicken breast tissue slice. The insets show the corresponding MIIPS traces. Note that even with the reduced signal to noise ratio caused by the presence of tissue, MIIPS is still able to characterize the spectral phase. (b) GDD introduced by a cow cornea-lens complex. The dashed zone in the inset shows the tissue used for the measurement. Aq. hum., aqueous humor; vit. hum., vitreous humor.

tions can be substantially minimized. Given that MIIPS is a single-beam method, mode quality plays no role as demonstrated in this subsection. The second contribution to noise comes from the detector. The results shown in Fig. 8(a) correspond to a 1:1 signal-to-noise ratio in the detected signal with minimal influence on the measured phase. Because MIIPS directly measures $\phi''(\omega)$, the integrated phase is relatively immune to noise in the measurement.

*3. Measurement of Complex Spectral Phases*

The availability of automated pulse shapers has made possible the generation of ultrashort laser pulses with complex spectral phases that are used in areas such as coherent control [20,40] and nonlinear microscopy [15,34,41]. The characterization of complex phases without the need of a well-characterized reference pulse has been experimentally demonstrated using MIIPS [16,19] and SPIDER [42]. Figure 9 shows examples of complex spectral phases measured by MIIPS. For these experiments, two independent all-reflective grating-based pulse shapers containing a 640 pixel dual-mask spatial light modulator (SLM-640, CRi Inc.) were used. One homemade pulse shaper introduced the desired spectral phase while the other (MIIPS Box 640 PA, BioPhotonic Solutions, Inc.) was used to measure it using MIIPS. The agreement between the introduced and measured phases illustrates the performance of the method for the case of complex spectral phases.

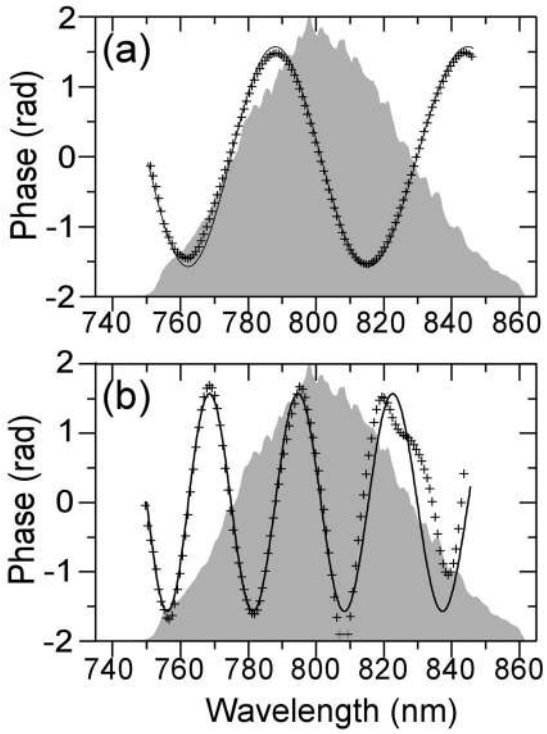


Fig. 9. MIIPS measurements of complex spectral phases. Synthetic spectral phases introduced by the first pulse shaper (solid curves). Phases measured by the MIIPS box (crosses). The shaded area represents the spectrum of the pulses. The introduced phases in (a) and (b) are sinusoidal functions with periods 39 and 78 fs, respectively.

### C. MIIPS Measurements With Other Nonlinear Optical Signals

Although the use of SHG for pulse characterization provides excellent results and great sensitivity, the required crystals can be expensive, introduce carrier-frequency and bandwidth limitations due to phase matching, and in addition, they have a limited wavelength range of operation. The following MIIPS implementations are free from these disadvantages because they do not require a frequency-doubling crystal.

*1. Surface-Second Harmonic Generation MIIPS*

Femtosecond lasers are increasingly being used for micromachining and other material processing applications. SHG occurring in the plasma generated during the ablation process in metallic and silicon surfaces has been shown to provide an excellent feedback signal for MIIPS [43]. This technique, surface-second harmonic generation multiphoton intrapulse interference phase scan (SSHG-MIIPS), has great potential for micromachining applications because pulse characterization is done at the point where machining actually occurs and any phase distortions, including those introduced by the microscope objective, can be corrected to achieve optimum and reproducible results without any change to the machining setup. Excellent agreement between SHG-MIIPS and SSHG-MIIPS measurements has also been shown [43]. Figure 10(a) shows SSHG-MIIPS traces of amplified pulses after spectral phase compensation.

*2. Air-MIIPS*

Third order harmonic generation (THG) in air is a practical alternative that is particularly useful for characterization and compression of intense femtosecond lasers. Excellent agreement between SHG-MIIPS and air-MIIPS measurements has been shown [44]. Figure 10(b) shows air-MIIPS traces of amplified pulses after spectral phase compensation.

*3. Self-Diffraction MIIPS*

Self-diffraction multiphoton intrapulse interference phase scan (SD-MIIPS) is currently under investigation in our laboratories. This method is particularly useful to characterize UV pulses for which SHG crystals are unavailable. Figures 10(c) and 10(d) show IR and UV SD-MIIPS traces. To obtain the SD we used a mask that blocked all but two small regions of the amplified output from our laser system. The resulting beams were then focused on the nonlinear medium, and the SD signal was detected using a compact fiber-coupled spectrometer. A 100 $\mu$m quartz plate and a 250 $\mu$m sapphire plate were used for the IR and UV pulses, respectively. For all cases TL pulses were used, except in Fig. 10(d), where a small quadratic and cubic dispersion is apparent in the spacing and angles of the features. These distortions can be corrected by measurement and compensation as discussed in this paper.

### D. Accurate Pulse Shaping

Pulse shapers have become important tools for controlling laser-driven processes. Feedback-optimized pulse shaping strategies have been shown in [45,46]. The approach we

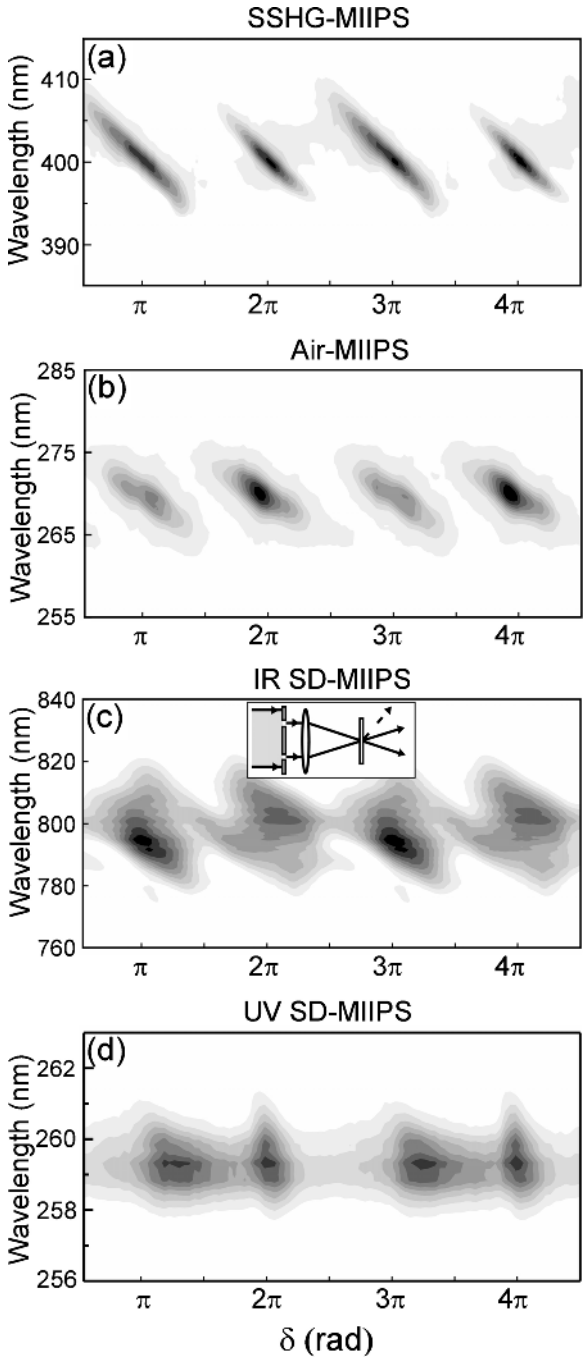


Fig. 10. Experimental traces of TL pulses obtained with different MIIPS implementations. (a) SSHG-MIIPS. The signal is produced in the plasma generated during the ablation process in a surface. The traces shown were generated from a Si wafer. (b) Air-MIIPS. The signal is obtained from THG in air. (c) IR SD-MIIPS and (d) UV SD-MIIPS. The signal is obtained by SD in a thin plate of nonlinear medium. The inset shows the experimental setup. The dashed line represents the SD beam. In cases (a)–(c), the parallel and equidistant features indicate TL pulses.

show here is based on an accurate correction of spectral phase distortions followed by the application of tailored phases using a well-calibrated pulse shaper. To illustrate the accuracy that can be achieved using this approach, we demonstrate remote characterization and shaping of ultrashort pulses.

*Pulse Characterization and Shaping for Standoff Applications.* Interest in applications requiring the propagation of amplified femtosecond laser pulses to a remote target has increased in recent years. Given that the laser-matter interaction is typically nonlinear in nature, the results and their reproducibility depend on the spectral phase of the laser pulses at the target. Therefore, accurate characterization and shaping of the pulses at the target are necessary for the success of these applications. A spectral phase measurement tens of meters away from the laser output requires dealing with special difficulties, such as poor beam pointing stability and mode quality, conditions that represent a significant challenge for most characterization techniques. Being a single-beam technique and independent of mode quality, MIIPS is ideal for standoff pulse characterization applications.

MIIPS has been shown to successfully characterize and shape amplified laser pulses ~30 m away from the exit aperture of the amplifier [47], a distance only limited by laboratory space. The method can in principle be used with targets placed kilometers away. More recently, standoff (>10 m) molecular identification was shown using single-beam coherent anti-Stokes Raman scattering (CARS) [31]. The method, which was originally introduced for microscopy [48], involves excitation and probing of molecular vibrations that work as chemical fingerprints and requires using polarization and spectral phase shaping to reduce the nonresonant background. Figure 11(a) shows the unprocessed single-beam CARS spectrum of toluene obtained at a ~12 m standoff distance between

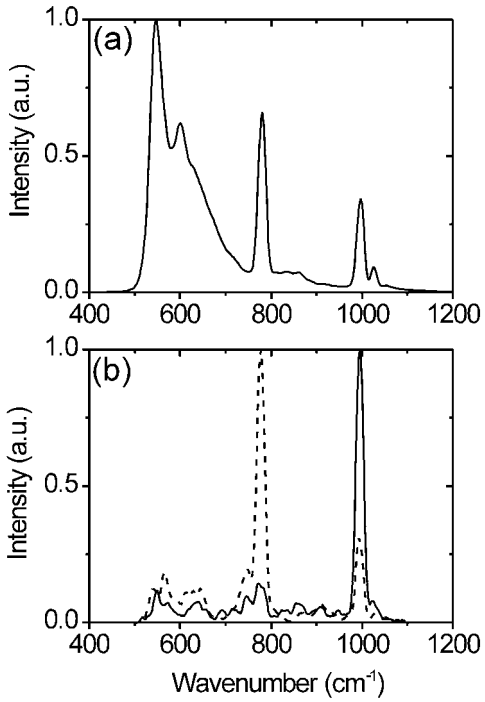


Fig. 11. Single-beam CARS spectra of toluene. (a) Unprocessed single-beam CARS spectrum of toluene. A large nonresonant background is present. (b) Unprocessed single-beam CARS spectra of toluene using specially designed pulses. For each spectrum, a binary phase designed to optimize individual excitation of vibrational modes was used. Selectivity and suppression of the nonresonant background were obtained. The spectra were obtained from a ~12 m standoff distance.

the laser and the detection system and the target. For single-beam CARS experiments, where a broad bandwidth is required, precompensation of the dispersion introduced by air is necessary (~20 $fs^2$/m at 800 nm [47]). Note that a considerable nonresonant background is present. Selective excitation of individual vibrational modes and elimination of the nonresonant background are demonstrated through optimal binary phase pulse shaping in Fig. 11(b).

## 4. OTHER PULSE SHAPER ASSISTED SPECTRAL PHASE CHARACTERIZATION METHODS

The presence of an adaptive pulse shaper in an optical setup eliminates the need of a separate device for pulse characterization. In addition to MIIPS, pulse shaper assisted versions of interferometric autocorrelation (IAC) and interferometric frequency resolved optical gating (IFROG) [49] have been implemented by introducing a nonlinear element in a single-beam setup [50]. A pulse shaper assisted collinear version of SPIDER (SAC-SPIDER) has also been demonstrated but still requires overlapping two beams [42]. In all of these cases, two identical replicas of the pulses to be measured, separated at various time delays $\tau$, need to be generated by applying a transfer function $M(\omega)=\cos[\omega\tau/2]$ to the pulse shaper [50].

Here, the laser system and adaptive pulse shaper described in [25] were used to implement chirp and sinusoidal MIIPS, shaper assisted versions of IAC, and its spectrally resolved counterpart IFROG. Note that for IAC, IFROG, and SAC-SPIDER, phase and amplitude shaping is required while for sinusoidal and chirp MIIPS only phase shaping suffices. Figure 12 shows the experimental traces corresponding to TL pulses compressed by MIIPS (left column) and 1500 $fs^3$ cubic phase shaped pulses (right column).

Beyond data acquisition, phase retrieval for each of these methods varies widely. In theory, IAC together with the spectrum of the pulses are sufficient to obtain the spectral phase by using an iterative algorithm [4]; however, experimental ambiguities have been reported [51]. IFROG requires Fourier transformations and a subsequent iterative algorithm, such as the conventional SHG-FROG, to retrieve the spectral phase [49]. The first derivative of the phase $\phi'(\omega)$ is obtained from a SPIDER interferogram using an algebraic procedure [42]. In sinusoidal MIIPS, the second derivative of the phase $\phi''(\omega)$ is calculated according to Eq. (2). For chirp MIIPS, no retrieval procedure is necessary because $\phi''(\omega)$ is directly visualized in the experimental trace [see Fig. 1(b)]. Note that in MIIPS one directly measures $\phi''(\omega)$, which is the function responsible for pulse broadening (Section 2).

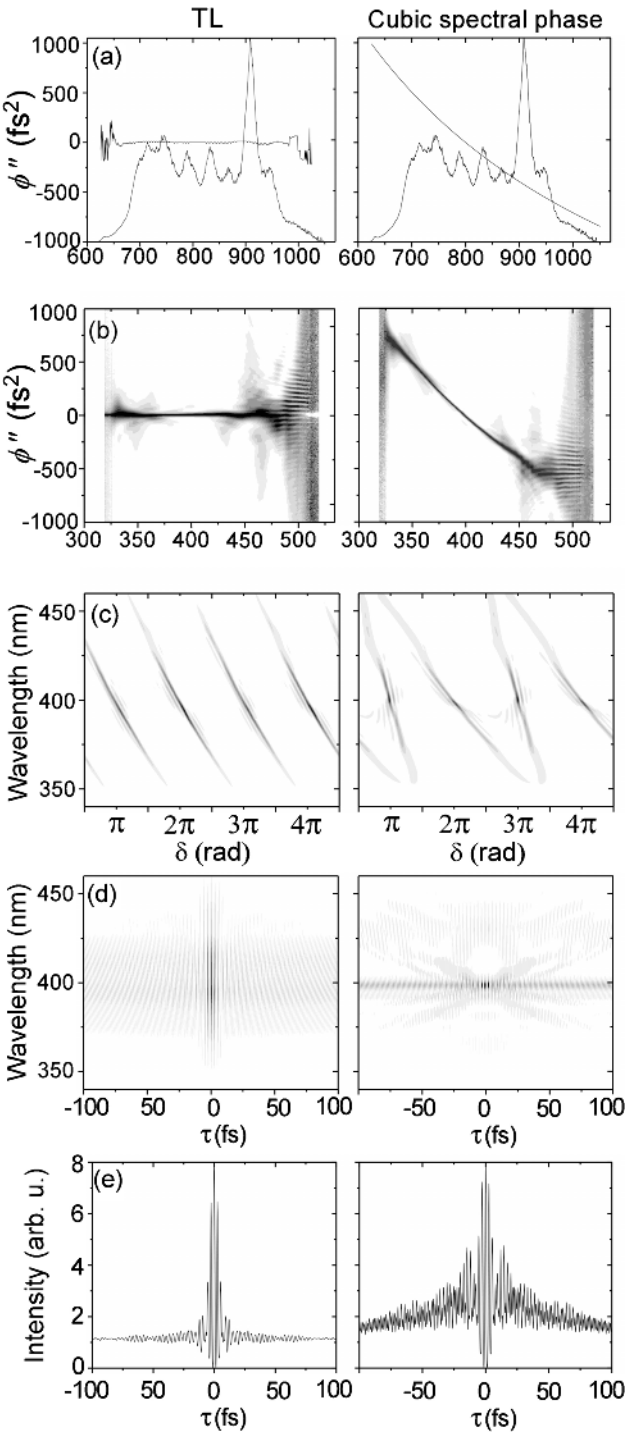


Fig. 12. Experimental traces obtained by different pulse shaper-based pulse characterization methods. (a) Spectrum and second derivative of the spectral phase of the pulses. (b) Chirp MIIPS, (c) sinusoidal MIIPS, (d) IFROG, and (e) IAC. The left and right columns correspond to a flat (TL) and a 1500 $fs^3$ cubic spectral phase, respectively.

## 5. CONCLUSIONS

In this paper, we have presented a number of MIIPS implementations for directly measuring $\phi''(\omega)$ without relying on phase retrieval algorithms. Data acquisition for MIIPS does not require autocorrelation, interferometry, or even a computer-controlled pulse shaper. When using a pulse shaper capable of accurately measuring the spectral phase of the pulses as shown here, it is straightforward to compensate the measured phase distortions. Compensation of phase distortions at the target is necessary for reproducible femtosecond laser applications.

Additional advantages of the MIIPS method were demonstrated with suitable examples. Dispersion measure-

ments of optical materials showed the accuracy of the method. Various possible implementations of the method using different nonlinear media demonstrated that MIIPS is conveniently versatile. Being insensitive to noise and beam quality, the method is quite robust and can be used even after scattering media, such as biological tissues and for applications requiring remote pulse shaping capabilities, where dust and clouds may be present. We are not aware of any other method capable of providing the full compensation of ~4 fs pulses as evidenced by the ~200 nm bandwidth SHG spectrum, the $\pm 0.2\ fs^2/mm$ accuracy in measurement of chromatic dispersion, and the wavelength independent flexibility during measurement and compensation of femtosecond laser pulses. These features make MIIPS ideal for applications in biomedical imaging, micromachining, standoff detection, and coherent control. The MIIPS technology is patent protected (U.S. patent 7,105,811 and other patents pending), licensed to BioPhotonic Solutions Inc. and Coherent Inc.

## ACKNOWLEDGMENTS

The projects that led to the results published herein were partially funded by a Major Research Instrumentation grant from the National Science Foundation CHE-0421047. Partial funding also comes from the Chemical Sciences, Geosciences, and Biosciences Division, Office of Basic Energy Sciences, Office of Science, U.S. Department of Energy. We are grateful for the original contribution to this work by J. M. Dela Cruz, D. A. Harris, H. Li, P. Xi, L. Weisel, P. Wrzesinski, and X. Zhu. We are also grateful for a number of fruitful discussions on pulse shaping and MIIPS with Igor Pastirk from BioPhotonic Solutions Inc.

## REFERENCES

1. R. L. Fork, C. H. B. Cruz, P. C. Becker, and C. V. Shank, "Compression of optical pulses to 6 femtoseconds by using cubic phase compensation," Opt. Lett. **12**, 483–485 (1987).
2. D. Yelin, D. Meshulach, and Y. Silberberg, "Adaptive femtosecond pulse compression," Opt. Lett. **22**, 1793–1795 (1997).
3. T. Baumert, T. Brixner, V. Seyfried, M. Strehle, and G. Gerber, "Femtosecond pulse shaping by an evolutionary algorithm with feedback," Appl. Phys. B: Lasers Opt. **65**, 779–782 (1997).
4. K. Naganuma, K. Mogi, and H. Yamada, "General-method for ultrashort light-pulse chirp measurement," IEEE J. Quantum Electron. **25**, 1225–1233 (1989).
5. R. Trebino and D. J. Kane, "Using phase retrieval to measure the intensity and phase of ultrashort pulses—frequency-resolved optical gating," J. Opt. Soc. Am. A **10**, 1101–1111 (1993).
6. R. Trebino, *Frequency-Resolved Optical Gating: The Measurement of Ultrashort Laser Pulses* (Kluwer Academic, 2000).
7. C. Iaconis and I. A. Walmsley, "Spectral phase interferometry for direct electric-field reconstruction of ultrashort optical pulses," Opt. Lett. **23**, 792–794 (1998).
8. C. Iaconis and I. A. Walmsley, "Self-referencing spectral interferometry for measuring ultrashort optical pulses," IEEE J. Quantum Electron. **35**, 501–509 (1999).
9. F. Verluise, V. Laude, Z. Cheng, C. Spielmann, and P. Tournois, "Amplitude and phase control of ultrashort pulses by use of an acousto-optic programmable dispersive filter: pulse compression and shaping," Opt. Lett. **25**, 575–577 (2000).
10. P. Baum, S. Lochbrunner, L. Gallmann, G. Steinmeyer, U. Keller, and E. Riedle, "Real-time characterization and optimal phase control of tunable visible pulses with a flexible compressor," Appl. Phys. B: Lasers Opt. **74**, S219–S224 (2002).
11. K. Yamane, Z. G. Zhang, K. Oka, R. Morita, M. Yamashita, and A. Suguro, "Optical pulse compression to 3.4 fs in the monocycle region by feedback phase compensation," Opt. Lett. **28**, 2258–2260 (2003).
12. H. X. Miao, A. M. Weiner, C. Langrock, R. V. Roussev, and M. M. Fejer, "Sensing and compensation of femtosecond waveform distortion induced by all-order polarization mode dispersion at selected polarization states," Opt. Lett. **32**, 424–426 (2007).
13. M. Dantus, V. V. Lozovoy, and I. Pastirk, "Measurement and repair: the femtosecond wheatstone bridge," OE Mag. **9**, 15–17 (2003).
14. V. V. Lozovoy, I. Pastirk, and M. Dantus, "Multiphoton intrapulse interference. IV. Ultrashort laser pulse spectral phase characterization and compensation," Opt. Lett. **29**, 775–777 (2004).
15. J. M. Dela Cruz, I. Pastirk, V. V. Lozovoy, K. A. Walowicz, and M. Dantus, "Multiphoton intrapulse interference 3: probing microscopic chemical environments," J. Phys. Chem. A **108**, 53–58 (2004).
16. B. Xu, J. M. Gunn, J. M. Dela Cruz, V. V. Lozovoy, and M. Dantus, "Quantitative investigation of the multiphoton intrapulse interference phase scan method for simultaneous phase measurement and compensation of femtosecond laser pulses," J. Opt. Soc. Am. B **23**, 750–759 (2006).
17. K. A. Walowicz, I. Pastirk, V. V. Lozovoy, and M. Dantus, "Multiphoton intrapulse interference. 1. Control of multiphoton processes in condensed phases," J. Phys. Chem. A **106**, 9369–9373 (2002).
18. V. V. Lozovoy, I. Pastirk, K. A. Walowicz, and M. Dantus, "Multiphoton intrapulse interference. II. Control of two- and three-photon laser induced fluorescence with shaped pulses," J. Chem. Phys. **118**, 3187–3196 (2003).
19. V. V. Lozovoy, B. Xu, Y. Coello, and M. Dantus, "Direct measurement of spectral phase for ultrashort laser pulses," Opt. Express **16**, 592–597 (2008).
20. V. V. Lozovoy and M. Dantus, "Coherent control in femtochemistry," Chem. PhysChem. **6**, 1970–2000 (2005).
21. Y. Coello, B. Xu, T. L. Miller, V. V. Lozovoy, and M. Dantus, "Group-velocity dispersion measurements of water, seawater, and ocular components using multiphoton intrapulse interference phase scan (MIIPS)," Appl. Opt. **46**, 8394–8401 (2007).
22. A. Baltuska and T. Kobayashi, "Adaptive shaping of two-cycle visible pulses using a flexible mirror," Appl. Phys. B: Lasers Opt. **75**, 427–443 (2002).
23. M. Yamashita, K. Yamane, and R. Morita, "Quasi-automatic phase-control technique for chirp compensation of pulses with over-one-octave bandwidth—generation of few- to monocycle optical pulses," IEEE J. Sel. Top. Quantum Electron. **12**, 213–222 (2006).
24. T. Binhammer, E. Rittweger, R. Ell, F. X. Kartner, and U. Morgner, "Prism-based pulse shaper for octave spanning spectra," IEEE J. Quantum Electron. **41**, 1552–1557 (2005).
25. B. Xu, Y. Coello, V. V. Lozovoy, D. A. Harris, and M. Dantus, "Pulse shaping of octave spanning femtosecond laser pulses," Opt. Express **14**, 10939–10944 (2006).
26. M. Hentschel, R. Kienberger, C. Spielmann, G. A. Reider, N. Milosevic, T. Brabec, P. Corkum, U. Heinzmann, M. Drescher, and F. Krausz, "Attosecond metrology," Nature **414**, 509–513 (2001).
27. Y. Oishi, A. Suda, K. Midorikawa, and F. Kannari, "Sub-10 fs, multimillijoule laser system," Rev. Sci. Instrum. **76**, 093114 (2005).
28. M. Nisoli, S. DeSilvestri, and O. Svelto, "Generation of high energy 10 fs pulses by a new pulse compression technique," Appl. Phys. Lett. **68**, 2793–2795 (1996).
29. M. Nisoli, S. DeSilvestri, O. Svelto, R. Szipocs, K. Ferencz, C. Spielmann, S. Sartania, and F. Krausz, "Compression of

high-energy laser pulses below 5 fs," Opt. Lett. **22**, 522–524 (1997).
30. Z. Cheng, A. Furbach, S. Sartania, M. Lenzner, C. Spielmann, and F. Krausz, "Amplitude and chirp characterization of high-power laser pulses in the 5-fs regime," Opt. Lett. **24**, 247–249 (1999).
31. H. Li, D. A. Harris, B. Xu, P. J. Wrzesinski, V. V. Lozovoy, and M. Dantus, "Coherent mode-selective Raman excitation towards standoff detection," Opt. Express **16**, 5499–5504 (2008).
32. I. Amat-Roldan, I. G. Cormack, P. Loza-Alvarez, and D. Artigas, "Starch-based second-harmonic-generated collinear frequency-resolved optical gating pulse characterization at the focal plane of a high-numerical-aperture lens," Opt. Lett. **29**, 2282–2284 (2004).
33. D. N. Fittinghoff, A. C. Millard, J. A. Squier, and M. Muller, "Frequency-resolved optical gating measurement of ultrashort pulses passing through a high numerical aperture objective," IEEE J. Quantum Electron. **35**, 479–486 (1999).
34. P. Xi, Y. Andegeko, L. R. Weisel, V. V. Lozovoy, and M. Dantus, "Greater signal, increased depth, and less photobleaching in two-photon microscopy with 10 fs pulses," Opt. Commun. **281**, 1841–1849 (2008).
35. A. G. Van Engen, S. A. Diddams, and T. S. Clement, "Dispersion measurements of water with white-light interferometry," Appl. Opt. **37**, 5679–5686 (1998).
36. A. H. Harvey, J. S. Gallagher, and J. Sengers, "Revised formulation for the refractive index of water and steam as a function of wavelength, temperature and density," J. Phys. Chem. Ref. Data **27**, 761–774 (1998).
37. M. Daimon and A. Masumura, "Measurement of the refractive index of distilled water from the near-infrared region to the ultraviolet region," Appl. Opt. **46**, 3811–3820 (2007).
38. W. Denk, J. Strickler, and W. Webb, "Two-photon laser scanning fluorescence microscopy," Science **248**, 73–76 (1990).
39. J. M. Dela Cruz, I. Pastirk, M. Comstock, V. V. Lozovoy, and M. Dantus, "Use of coherent control methods through scattering biological tissue to achieve functional imaging," Proc. Natl. Acad. Sci. U.S.A. **101**, 16996–17001 (2004).
40. V. V. Lozovoy and M. Dantus, "Laser control of physicochemical processes; experiments and applications," Annu. Rep. Prog. Chem., Sect. C: Phys. Chem. **102**, 227–258 (2006).
41. J. P. Ogilvie, D. Debarre, X. Solinas, J. L. Martin, E. Beaurepaire, and M. Joffre, "Use of coherent control for selective two-photon fluorescence microscopy in live organisms," Opt. Express **14**, 759–766 (2006).
42. B. von Vacano, T. Buckup, and M. Motzkus, "Shaper-assisted collinear SPIDER: fast and simple broadband pulse compression in nonlinear microscopy," J. Opt. Soc. Am. B **24**, 1091–1100 (2007).
43. X. Zhu, T. C. Gunaratne, V. V. Lozovoy, and M. Dantus, "In-situ femtosecond laser pulse characterization and compression during micromachining," Opt. Express **15**, 16061–16066 (2007).
44. D. A. Harris, J. C. Shane, V. V. Lozovoy, and M. Dantus, "Automated phase characterization and adaptive pulse compression using multiphoton intrapulse interference phase scan in air," Opt. Express **15**, 1932–1938 (2007).
45. T. Brixner, A. Oehrlein, M. Strehle, and G. Gerber, "Feedback-controlled femtosecond pulse shaping," Appl. Phys. B: Lasers Opt. **70**, S119–S124 (2000).
46. D. Meshulach, D. Yelin, and Y. Silberberg, "Adaptive real-time femtosecond pulse shaping," J. Opt. Soc. Am. B **15**, 1615–1619 (1998).
47. I. Pastirk, X. Zhu, R. M. Martin, and M. Dantus, "Remote characterization and dispersion compensation of amplified shaped femtosecond pulses using MIIPS," Opt. Express **14**, 8885–8889 (2006).
48. D. Oron, N. Dudovich, and Y. Silberberg, "Femtosecond phase-and-polarization control for background-free coherent anti-Stokes Raman spectroscopy," Phys. Rev. Lett. **90**, 213902 (2003).
49. G. Stibenz and G. Steinmeyer, "Interferometric frequency-resolved optical gating," Opt. Express **13**, 2617–2626 (2005).
50. A. Galler and T. Feurer, "Pulse shaper assisted short laser pulse characterization," Appl. Phys. B: Lasers Opt. **90**, 427–430 (2008).
51. J. H. Chung and A. M. Weiner, "Ambiguity of ultrashort pulse shapes retrieved from the intensity autocorrelation and the power spectrum," IEEE J. Sel. Top. Quantum Electron. **7**, 656–666 (2001).